7th International Conference on the Durability of Concrete Structures
20-22 May 2022
University of Jinan, Jinan, Shandong, China

Rheological properties and structural build-up of 3D printed magnesium potassium phosphate cement

Zhihui Zhao, Yuan Jin, Jun xu, Lingchao Lu*

Shandong Provincial Key Lab. of Preparation and Measurement of Building Materials, University of Jinan, Jinan 250022, China

*Corresponding author: E-mail: lingchao_lu@163.com (L. Lu);

ABSTRACT

This paper focuses on the rheological properties of 3D printed magnesium potassium phosphate cements (MKPCs) with different magnesium-to-phosphate (M/P) mass ratio, MgO fineness and supplementary cementitious materials (SCMs) types. The variable shear rate tests were used to monitor the extrudability. The highest slope of the evolution of storage modulus (G') and the maximum static yield stress (M_{TS}) value were used as an indication of the rigidification rate. The increased M/P mass ratio, MgO fineness and SCMs addition resulted in the promoted structural build-up of 3D printed MKPCs. The consistency between the evolution of G' and Mτs with elapsed time were observed and the comparable time values of tg and t_{MTS} were obtained. XRD results indicate the reversible agglomeration at the very early minutes can be ascribed to the solely physical flocculation changes other than the new hydration product.

NOTATION

G' storage modulus
δ phase angle
τ_S static yield stress
$\dot{\gamma}$ shear rate
t_g the characteristic time of highest slope of G' curve
$t_{\delta=45^\circ}$ the characteristic time of δ = 45°
M_{TS} the maximum τ_S value
t_{MTS} the characteristic time of M_{TS}

1. INTRODUCTION

Extrusion-based 3D printing with concrete (3DPC), as a promising additive manufacturing has drawn the focused attention in construction industry [1-3]. Despite the superior advantages of 3DPC in delivering high construction efficiency and less labor consumption [4-6], a major factor for successful application of 3DPC in construction is the printable cementitious materials should meet the rheological requirements [7]. The requirements between different processes highlight the importance of the rapid hardening cementatious materials [8, 9] for a successful 3DPC. One of the promising alternative is magnesium potassium phosphate cements (MKPCs), synthesized by magnesia and phosphate salts [10]. Nevertheless, limited attention has been paid on the rheological behaviors of MKPCs concerning 3D printing.

In this study, the influence of M/P mass ratio, MgO fineness and the addition of SCMs on the rheological behaviors of MKPCs were studied. The dynamic yielding properties were monitored by variable shear rate test. The time evolution of storage modulus (G'), phase angle (δ) and static yield stress (τ_S) were investigated to describe the structural build-up of the mixture at rest. The composition of the reversible agglomeration in the very early age was analyzed by XRD.

2. MATERIALS

The mixtures were prepared with the dead-burned magnesia, analytical grade KH_2PO_4 and borax ($Na_2B_4O_7$•$5H_2O$.), using a water/binder ratio (W/B) of 0.14. Also, three types of SCMs, namely metakaolin (MK), ground granulated blast furnace slag (GBFS) and silica fume (SF) were employed to partially replace the acidic and alkali components to make the mixtures more “printable”. The particle size

distribution of different fineness of MgO is given in Fig. 1.

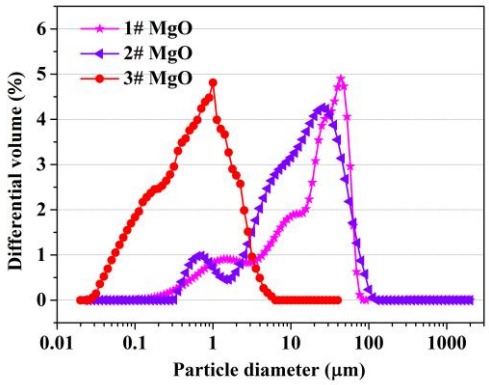

Figure 1. The particle size distributions of magnesia.

3. RHEOLOGICAL METHODS

3.1 VARIABLE SHEAR RATE TEST

The HAAKE MARS 40 rheometer is adopted in this study. The variable shear rate test procedure consists of pre-shear at 50 s^{-1} for 60 s and rested for 60 s, followed by the variable shear rate of 0-100 s^{-1} (100-0 s^{-1}). Dynamic yield stress and plastic viscosity were determined as the y-intercept and slope from the ramp down flow curves that satisfactorily fit to the Bingham model, respectively, given by Eq. (1).

Bingham model: $\tau=\tau_0+\mu\dot{\gamma}$ Eq. (1)

Where μ is the plastic viscosity (Pa.s), τ is the shear stress (Pa), τ_0 is the yield stress (Pa) and $\dot{\gamma}$ is the shear rate.

3.2 TIME SWEEP TEST

Then the time evolution of visco-elastic properties (G' and δ) were conducted to evaluate the structural build-up of the printed layers in this study. Fig. 2 shows the time sweep testing procedure.

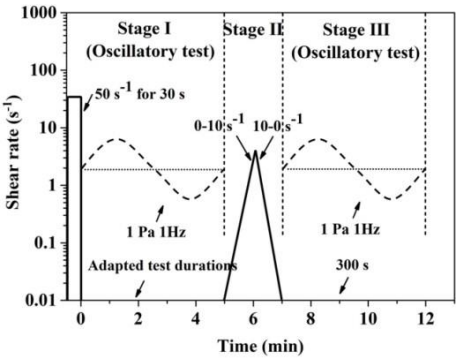

Figure 2. The time sweep testing procedure.

3.3 STATIC YIELD STRESS

Trial tests have been conducted on each mixture. The more flowable mixtures with M/P ratio of 2.0 and 2.5 started at 10 min while less flowable mixtures with M/P ratio of 3.0 and 3.5 started at 6 min were determined. The evolution of τ_S with elapsed time tests are comprised of Stage I and Stage II, as demonstrated in Fig. 3b. In Stage I, remix the material with the shear rate of 10 s^{-1} for 120 s before each resting period to achieve a fully broken state. But, the remix procedure was not applied again in the Stage II so as to determine the increase rate of τ_S related to the real deposition of printed layers accurately.

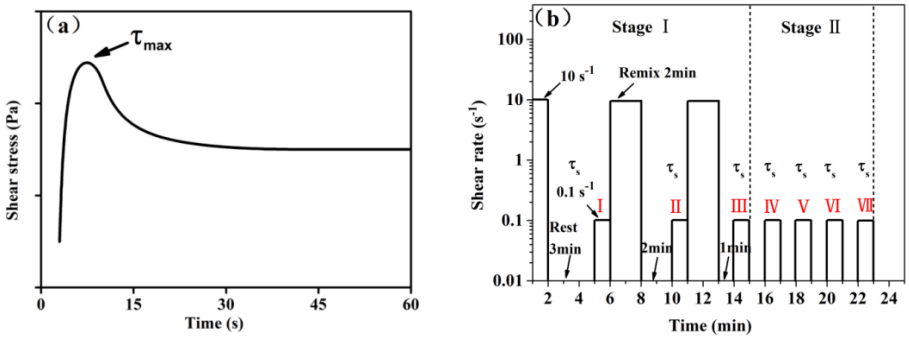

Figure 3. (a) Peak value represents the static yield stress and (b) the testing procedure.

4. RESULTS AND DISCUSSION

4.1 PUMPABILITY-DYNAMIC YIELD STRESS AND PLASTIC VISCOSITY

Table 1 shows the dynamic yield stress and plastic viscosity results of mixtures fitted from the ramp down

flow curves according to the Bingham model. The increased M/P mass ratio, MgO fineness and SCMs addition led to the promoted dynamic yield stress and slightly increased plastic viscosity, which can be ascribed to the stronger inter-particle interactions in mixtures. The promoted dynamic yield stress is conducive to the buildability without blocking the pipe during extrusion.

4.2 BUILDABILITY-TIME SWEEP TEST

The less flowable a material is, the longer rest time it takes to reach the peak value of modulus evolution curve. The adapted duration times for mixtures with M/P ratio of 2.0, 2.5, 3.0 and 3.5 are determined as 420 s, 840 s, 300 s and 300 s, respectively, as described in Table 2.

Table 1. Dynamic yield stress and plastic viscosity results of mixtures fitted by the Bingham model

Parameters	Mixture	Dynamic yield stress (Pa)	Plastic viscosity (Pa.s)
M/P mass ratio	2.0	4.981	2.876
	2.5	41.458	4.064
	3.0	33.941	4.978
	3.5	32.791	6.905
MgO fineness	1#	47.642	5.861
	2#	33.941	4.978
	3#	251.911	15.718
SCMs	10% MK	31.479	6.710
	20% MK	67.691	10.013
	30% MK	256.057	13.347
	30% SF	351.374	18.730
	30% GBFS	518.610	12.675

Note: t_g is the characteristic time of highest slope of G' curve; $t_{\delta=45^\circ}$ is the characteristic time of δ = 45°; M_{T_S} is the maximum τ_S value; $t_{M_{T_S}}$ is the characteristic time of M_{T_S}.

Fig. 4a and Fig. 4b show the evolution of G' and δ with elapsed time of mixtures with different M/P ratio, respectively. The inflection points (t_g) marked with the crosses presenting the highest slope of variation of G' accounts for the very fast formation of reversible agglomeration are presented in Fig. 3a. The times where the t_g occurred for mixtures with M/P ratio of 2.0, 2.5, 3.0 and 3.5 were at 21 min, 16 min, 11 min and 7 min, respectively, indicating that the increase in M/P ratio resulted in the sharp increase of G' and faster formation of the reversible agglomeration. After remix the mixture with the variable shear rate, the mixture exhibited a decreased G' as the structure broke down. Then the G' increased again rapidly at first few minutes and maintained at a high level when the mixtures were allowed to rest during the repeated time sweep tests.

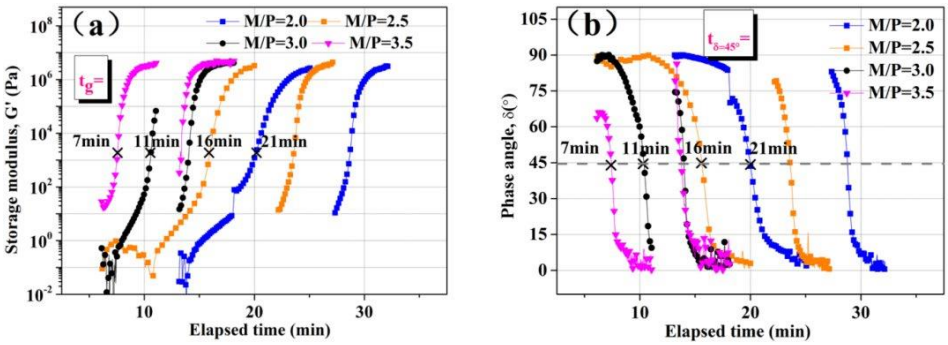

Figure 4. Evolution of (a) storage modulus and (b) phase angle with elapsed time for mixtures with different M/P ratio.

The evolution of δ with elapsed time is presented in Fig. 5b. The δ was calculated as phase angle (tan δ=G"/G') and it is closely related to the visco-elastic properties of the mixture. The value of 45° corresponds to the transition from viscous state to elastic state. It can be seen the times where δ = 45° ($t_{\delta=45^\circ}$) occurred for mixtures with M/P ratio of 2.0, 2.5, 3.0 and 3.5 were coincide at 21 min, 16 min, 11 min and 7 min, respectively.

Fig. 5 presents the time development of G' and δ of mixtures with different MgO fineness. The times where the t_g occurred for mixtures with 1# MgO, 2# MgO and 3# MgO were at 26 min, 11 min and 7 min, respectively, indicating that the increase in MgO fineness resulted in the shorter inter-particle distances and consequently a faster formation of the reversible structure. In similar, the $t_{\delta=45^\circ}$ occurred for mixtures with 1# MgO, 2# MgO and 3# MgO were at 28 min, 11 min and 10 min, respectively.

Fig. 6a and Fig. 6b show the time evolution of G' and δ of mixtures with different types of 30% SCMs, respectively. Mixtures with 30% SCMs exhibited relatively earlier time of $t_{\delta=45^\circ}$ at 7 min than the control of 11 min and it was more significant by 30%

MK addition than that of 30% GBFS addition. No matter what type of SCMs is added, a shorter induction period and an accelerated structural build-up are observed.

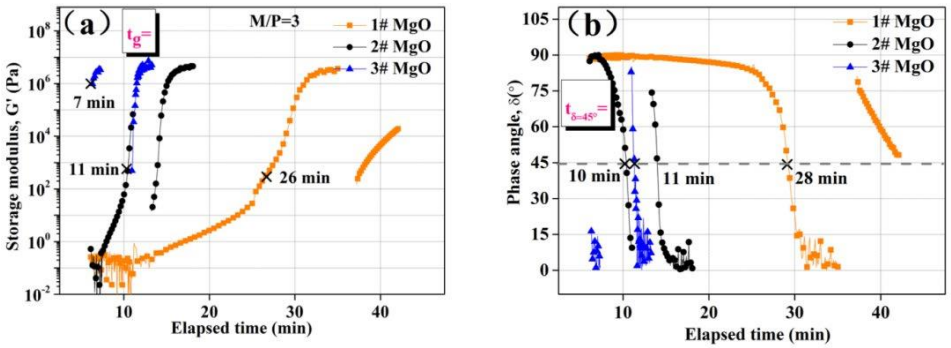

Figure 5. Evolution of (a) storage modulus and (b) phase angle with elapsed time for mixtures with different MgO fineness.

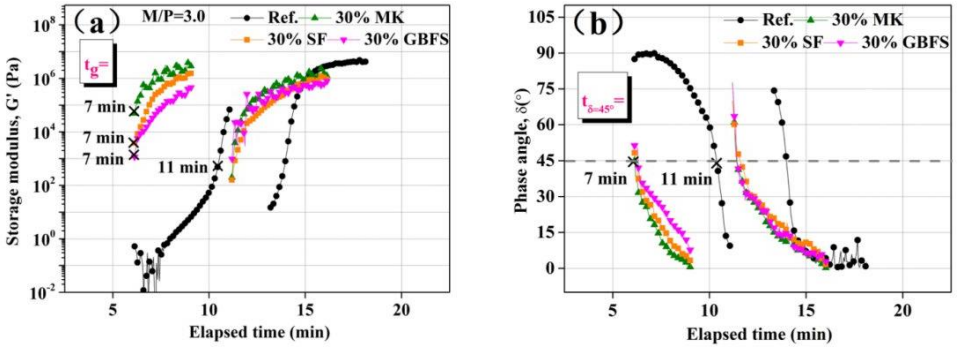

Figure 6. Evolution of (a) storage modulus and (b) phase angle with elapsed time for mixtures with different types of 30% SCMs.

4.3 BUILDABILITY-STATIC YIELD STRESS

The time evolution of τ_S is another effective method to characterize the structural build-up of 3D printed MKPCs. Fig. 7 shows the variation of τ_S with elapsed time for mixtures with different M/P ratio. The maximum τ_S value ($M_{\tau S}$) occurred for mixtures with M/P ratio of 2.0, 2.5, 3.0 and 3.5 were at 27 min, 16 min, 12 min and 12 min, respectively, indicating the earlier formation of reversible agglomeration in mixtures with high M/P ratio.

Fig. 8 shows the $t_{M\tau S}$ occurred for mixtures with 1# MgO, 2# MgO, 3# MgO and 30% MK were at 33 min, 12 min, 12 min and 12 min, respectively. The $t_{M\tau S}$ results were found to be consistent with the time sweep test results and the comparable time values of tg and $t_{\delta=45^\circ}$ were tested.

It can be concluded that the increased M/P mass ratio, MgO fineness and SCMs addition resulted in the promoted structural build-up. The decrease in inter-particles distances promotes the formation of reversible flocculation and hydration bonds between particles. Structural build-up of mixtures at rest can be related to the combined effects of physical and chemical changes [11, 12].

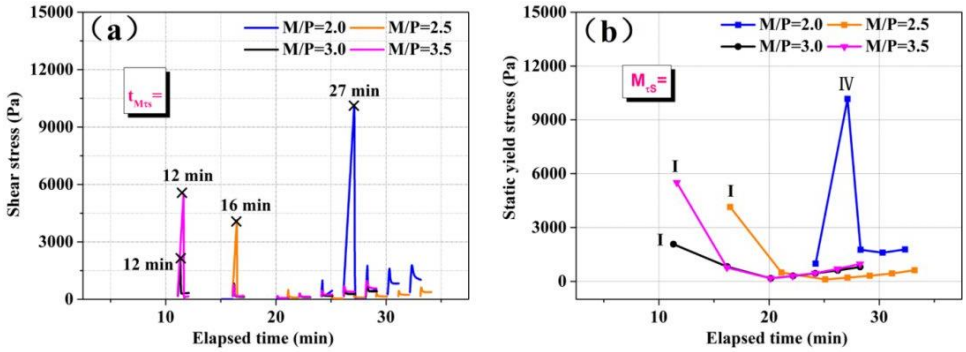

Figure 7. Evolution of (a) shear stress and (b) static yield stress with elapsed time for mixtures with different M/P ratio.

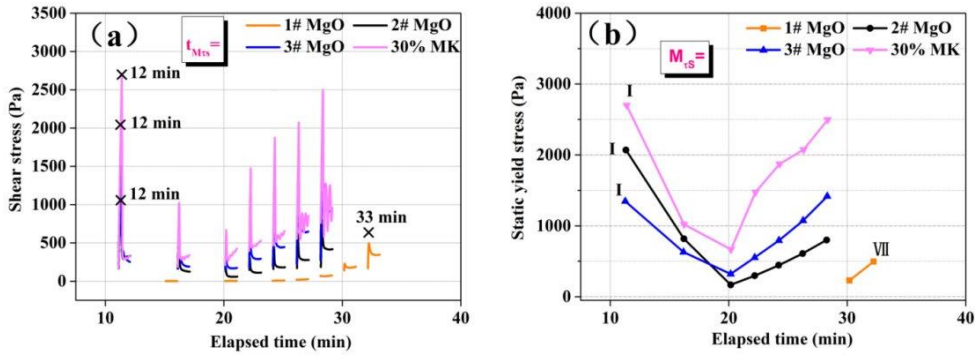

Figure 8. Evolution of (a) shear stress and (b) static yield stress with elapsed time for mixtures with different MgO fineness and 30% MK.

4.4 XRD TEST

To understand the composition of reversible agglomeration, Fig. 9 shows the XRD patterns of hydrates at 10 min age. The peaks of K-struvite ($MgKPO_4•6H_2O$) and unreacted MgO are detected. Although attempts to investigate the reversible agglomeration had been made, it is still difficult to elucidate the composition of it. And the fast development of G' (δ) of 3D printed MKPCs observed in the very early age can be ascribed to the solely physical flocculation changes other than the new hydration product, as supposed.

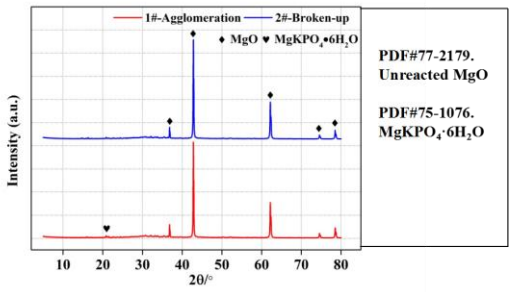

Figure 9. XRD patterns of reversible agglomeration and the broken-up mixture at 10 min age.

5. CONCLUSIONS

This paper focused on the the dynamic yielding property and the structural build-up of 3D printed MKPCs with respect to the factors of M/P mass ratio, MgO fineness and addition of SCMs. It can be concluded:

The highest slope of the evolution of G' and the maximum static yield stress can be used as an indication of the rigidification rate, indicating the formation of reversible agglomeration in mixtures at the first few minutes.

The increased M/P mass ratio, MgO fineness and SCMs addition advanced the time of G' and t_{MTS} occured and increased the structural build-up of mixture, making MKPCs a promising candidate for 3D printing.

The consistency between the evolution of G' and T_S with elapsed time were observed and the comparable time values were obtained.

XRD result shows the reversible agglomeration of 3D printed MKPCs observed in the very early age can be ascribed to the solely physical flocculation changes other than the new hydration product.

ACKNOWLEDGEMENTS

This research was funded by the Natural Science Foundations of China under grant number of 52072147.

CONFLICTS OF INTEREST

There is no conflict of interest.

REFERENCES

1. Salet T.A., Ahmed, Z.Y., Bos, F.P., Laagland, H.L., 2018. Design of a 3D printed concrete bridge by testing. Virtual and Physical Prototyping, 1-15.
2. Paolini, A., Kollmannsberger, S., Rank, E., 2019. Additive manufacturing in construction: a review on processes, applications, and digital planning method. Additive Manufacturing, 30:100894.
3. Buswell, R. A., Leal de Silva, W.R., Jones,S.Z., 2018. Dirrenberger, 3D printing using concrete extrusion: a road map for research. Cement and Concrete Research, 112:37-49.
4. Wangler, T., Roussel, N., Bos, F.P., Salet, T.A.M., Flatt, R.J., 2019. Digital concrete: a review. Cement and Concrete Research, 123:105780.
5. Bhattacherjee, S., Basavaraj, A.S., Rahul, A.V., Santhanam, M., Gettu, R., Panda, B., Schlangen, E., Chen, Y., Copuroglu, O., Ma, G., Wang, L., Beigh, M.A.B., Mechtcherine, V., 2021. Sustainable materials for 3D concrete printing. Cement and Concrete Composition, 122:104156.
6. Adaloudis, M., Bonnin Roca, J., 2021. Sustainability tradeoffs in the adoption of 3D Concrete Printing in the construction industry. Cement and Concrete Composition, 307:127201.
7. Le, T.T., Austin, S.A., Lim, S., Buswell, R.A., Gibb, A.G.F., Thorpe, T., 2012. Mix design and fresh properties for high-performance printing concrete. Material Structure, 45:1221-1232.
8. Khalil, N., Aouad, G., El Cheikh, K., Rémond, S., 2017. Use of calcium sulfoaluminate cements for setting control of 3D-printing mortars. Construction and Building Material, 157:382-391.
9. Chen, M., Liu, B., Li, L., Cao, L., Huang, Y., Wang, S., Zhao, P., Lu, L., Cheng, X., 2020. Rheological parameters, thixotropy and creep of 3D-printed calcium sulfoaluminate cement composites modified by bentonite. Composites Part B Engineering, 186:107821.
10. Lu, Z., Hou, D., Ma, H., Fan, T., Li, Z., 2016. Effects of grapheme oxide on the properties and microstructures of the magnesium potassium phosphate cement paste. Construction and Building Material, 119:107-112.
11. Mostafa, A.M., Yahia, A., 2017. Physico-chemical kinetics of structural build-up of neat cement-based suspensions. Cement and Concrete Research, 97:11-27.
12. Roussel, N., Ovarlez, G., Garrault, S., Brumaud, C., 2012. The origins of thixotropy of fresh cement pastes. Cement and Concrete Research, 42:148-157.